UDC 621.372.543.2.029.65: 621.372.852.1
Indexing Terms: Electric filters, bandpass, Waveguide components

Optimized low-insertion-loss millimetre-wave fin-line and metal insert filters

J. BORNEMANN, Dipl. Ing.,*
R. VAHLDIECK, Dipl.Ing.,*
Professor F. ARNDT, Dr.-Ing.*
and
D. GRAUERHOLZ, Dipl.Ing.*

SUMMARY

Low passband insertion-loss is achieved (1) by large-gap fin-lines, by which the high-Q potential increasing with gap-width is fully utilized, and (2) by pure metal inserts mounted in the E-plane of rectangular waveguides requiring no supporting dielectrics. This design combines the advantages of low-cost etching techniques and the low-loss performance of usual waveguide circuits. The theory described includes both higher-order mode interaction of the discontinuities and the finite thickness of dielectrics, metal fins as well as inserts. An optimizing computer program varies the filter parameters for a given number of resonators until the insertion loss yields a minimum in passband and an optimum in stopband. Data for optimized X-, Ka-, V-, E-, and W-band filters are given. Measurements verify the described theory. Measured minimum pass-band insertion losses are 0·3, 0·7, 1·5 dB for the fin-line filter for midband frequencies of about 12, 34, 75 GHz, and for the metal insert filter 0·1, 0·6, 0·5, and 0·7 dB at 12, 33, 63, and 76 GHz, respectively.

* *Microwave Department, University of Bremen, Kufsteiner Str. NW 1, D-2800 Bremen 33, West-Germany*

1 Introduction

In a fin-line structure,[1-14] metal inserts ('fins') are printed on a dielectric substrate (Fig. 1(a)), mounted in the E-plane of a rectangular waveguide. Besides the advantages of low-cost production through batch-processing techniques the fin-line configuration offers the potential for low-insertion loss filter designs if extremely high gap widths g (equal to the height b of the waveguide housing) are taken into account.[12,13] The reason is that the quality factor increases with increasing gap width, the optimum value being reached for the gap width $g = b$. (Ref. 2).

Low insertion-losses secondly result from a complete absence of supporting (lossy) dielectrics.[15-20] For the filter structure of Fig. 1(b) therefore the design is restricted to pure metal inserts, suitable for metal stamping or etching techniques, placed in the E-plane of rectangular waveguides.

For these two millimetre low-insertion-loss filter types design examples have been based on experimental data,[2,16,17] on equivalent-circuit theories,[18,19] and on an equivalent-waveguide approach.[5-7] These design methods neglect the higher-order-mode interaction which reduces the stopband insertion loss, or the finite thicknesses of substrates and inserts, which influence midband frequency, as well as ripple behaviour in the passband, and the stopband insertion-loss. Recently a design theory has been introduced by the

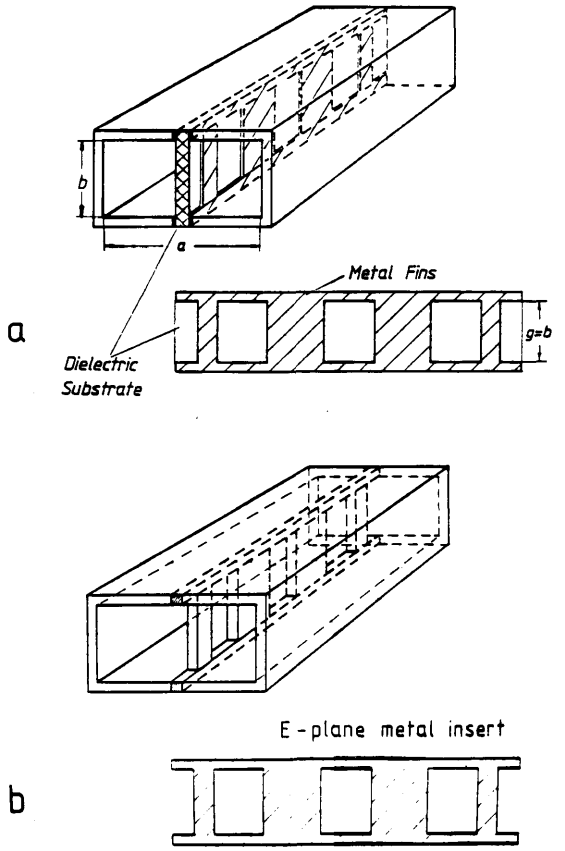

Fig. 1. Low-insertion-loss filter structures. (a) large gap fin-line filter; (b) E-plane metal insert filter.

0033-7722/82/110513+09 $1.50/0

authors,[12,13,20] which includes both higher-order-mode interaction and finite thicknesses of substrates and metal inserts.

The purpose of this paper is to present new design examples, calculated with the method of Refs. 12, 13 and 20, and to compare the low-insertion-loss fin-line filter results with those of the pure metal insert filter. It will be shown that measured minimum insertion-losses in the passband are 0·3, 0·7, 1·5 dB for the fin-line filter at midband frequencies of about 12, 34, 75 GHz, and 0·1, 0·6, 0·5, 0·7 dB for the metal insert filter at 12, 33, 63, and 76 GHz, respectively.

Since millimetre-wave components require direct waveguide implementation, higher-order-mode excitation problems at the discontinuities are of great interest. For three typical waveguide discontinuities, waveguide with an E-plane metal insert of finite length, waveguide with a dielectric-slab structure mounted in the E-plane, and the abrupt transition waveguide to a shielded microstrip-line, the fundamental and higher-order-mode scattering parameters are calculated and compared with each other.

Further, the computer optimization method for the filter design is described. The optimization is based on an evolution strategy method,[21] where no differentiation steps are required. This reduces the involved computation time compared with commonly used methods, e.g. the Fletcher-Powell procedure.[22]

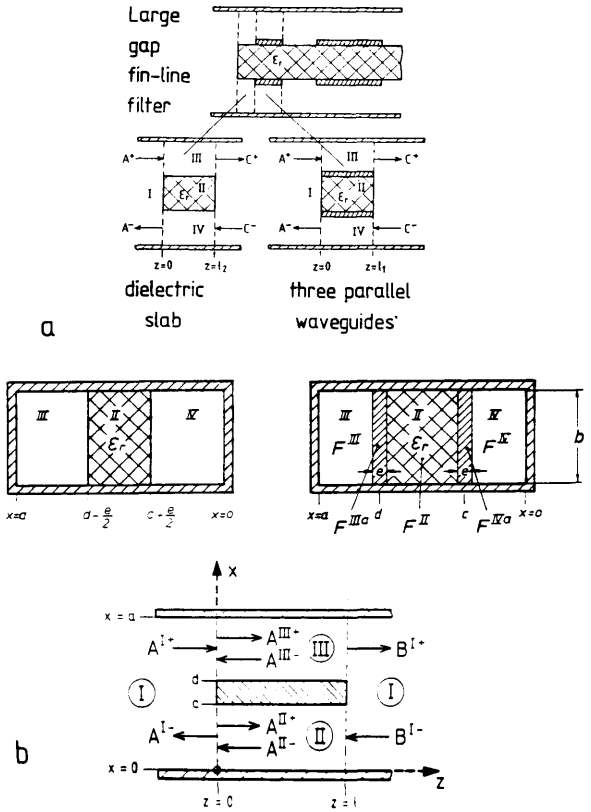

Fig. 2. Configuration for the field theory treatment. (a) fin-line structure (alternating three waveguides and dielectric-slab structure); (b) metal insert structure.

2 Theory

Since the theory is already explained in Ref. 12, its description can be abbreviated here and only the main aspects are elucidated. The fin-line filter (Fig. 1(a)) is regarded as consisting of alternating waveguide structure types: a waveguide with a dielectric slab and three parallel waveguides, the middle of which is filled with the same dielectric (Fig. 2(a)). The scattering matrices of each discontinuity are calculated including higher-order-mode excitation; the scattering matrix of the total fin-line structure is then obtained by suitably combining the transitions.

The metal insert filter (Fig. 1(b)) can be calculated by reducing the dielectric substrate thickness of the fin-line filter (Fig. 1(a)) to a negligible small value, or by directly calculating the simpler structure (Fig. 2(b)). The results are equivalent as has been proved in Ref. 20. In this paper only the first method is presented.

For the three waveguides structure of the fin-line filter in each subregion v = I, II, III, IV (Fig. 2(a)) the fields[23]

$$\mathbf{E}^{(v)} = -j\omega\mu\nabla X\boldsymbol{\Pi}_{hx}^{(v)},\quad \mathbf{H}^{(v)} = \nabla X\nabla X\boldsymbol{\Pi}_{hx}^{(v)} \tag{1}$$

are derived from the x-component of the magnetic Hertzian vector potential $\boldsymbol{\Pi}_{hx}$ which is assumed to be a sum of suitable eigenmodes satisfying the vector Helmholtz equation[23]

$$\nabla^2\boldsymbol{\Pi}_h + k^2\boldsymbol{\Pi}_h = 0,\qquad k^2 = \omega^2\mu\varepsilon \tag{2}$$

and the boundary conditions at the metallic surfaces:

$$\boldsymbol{\Pi}_{hx}^{(v)} = \sum_{m=1}^{\infty} A_m^{(v)\pm}\sin\left(\frac{m\pi}{p^v}\cdot f^v\right)\exp\left(\mp jk_{zm}^v z\right) \tag{3}$$

The propagation factor k_{zm}^v and the abbreviations p^v, f^v are explained in the Appendix. $A_m^{(v)\pm}$ are the still unknown eigenmode amplitudes of the forward and backward waves which are suitably normalized to the related power so that the power carried by a given wave is proportional to the square of the wave-amplitude coefficients. This leads directly to the desired scattering parameters.

By matching the transversal field components $\mathbf{E}_t$ and $\mathbf{H}_t$, which are given by (1) and (3), at the common interfaces F^{III}, F^{IIIa}, F^{II}, F^{IVa}, F^{IV} (Fig. 2a) across the step discontinuity at $z = 0$ the coefficients $A^{(v)\pm}$ in (3) can be related to each other after multiplication with the appropriate orthogonal function, which leads to the coupling integrals given in the Appendix. If the forward and backward waves at the two steps ($z = 0$ and $z = l_2$, Fig. 2(a)) of the structure of finite length l_2 are suitably related together, then (1)–(3) can be written as the desired scattering matrix

$$\begin{pmatrix}(A^-)\\(C^+)\end{pmatrix} = \begin{pmatrix}(S_{11})(S_{12})\\(S_{21})(S_{22})\end{pmatrix}\begin{pmatrix}(A^+)\\(C^-)\end{pmatrix}. \tag{4}$$

For details the reader is referred to Ref. 12.

The dielectric slab structure is treated in a similar manner. The common propagation factor k_{zm} in regions II, III, and IV is determined by the boundary conditions along the dielectric slab. A system of linear equations is obtained where the determinant is required to be zero. This leads to a transcendental equation which is solved numerically.[12]

The scattering matrix of the total fin-line structure is obtained by suitably combining the transitions, the length of waveguide I (Fig. 2(a)) being reduced to zero if the structures are joined together directly. A series of steps is commonly treated by transmission matrix parameters. But this is not appropriate if, like here, higher-order modes are included which are excited below their cut-off frequency. Since transmission matrix parameters for certain frequencies may then contain exponential functions with positive argument they exceed for many geometrical cases the available numerical range of the computer. The direct combination, however, of the resulting scattering matrices $(S)^{I}$, (S^{II}) is numerically stable as is shown for two steps I and II as an example, only containing exponential functions with negative arguments

$$\begin{bmatrix} b^{I} \\ b^{II} \end{bmatrix} = \left(\begin{bmatrix} S^{I}_{11} & 0 \\ 0 & S^{II}_{22} \end{bmatrix} + \begin{bmatrix} S^{I}_{12}D & 0 \\ 0 & S^{II}_{21}D \end{bmatrix} \times \right.$$
$$\left. \times \begin{bmatrix} ES^{II}_{11}D & E \\ F & FS^{I}_{22}D \end{bmatrix} \begin{bmatrix} S^{I}_{21} & 0 \\ 0 & S^{II}_{12} \end{bmatrix} \right) \begin{bmatrix} a^{I} \\ a^{II} \end{bmatrix}, \quad (5)$$

where I and II denote the steps I and II, respectively, and

$$E = (U - S^{II}_{11}DS^{I}_{22}D)^{-1}$$

$$F = (U - S^{I}_{22}DS^{II}_{11}D)^{-1},$$

a = incident waves, b = scattered waves, U = unit matrix, D = diagonal matrix with

$$D_{ii} = \exp(-\gamma_i l_i)$$

due to the section lengths l_i with the propagation constants γ_i between the step discontinuities. A series of more than two discontinuities can be treated in an analogous manner to (5).

3 Scattering Parameters of E-plane and H-plane Waveguide Discontinuities

Millimetre-wave components require direct waveguide implementation. As a first result of the given theory, therefore, the magnitude of the fundamental and higher-order mode transmission coefficients (scattering parameters $|S_{21}|$, eqn. (4)) is shown as a function of frequency of the complete discontinuity of a metal insert structure with finite length in the E-plane of a rectangular waveguide (Fig. 3). It can be stated that the power transmitted along the discontinuity is carried by H_{m0}-modes which are well compatible with the incident H_{10}-mode.

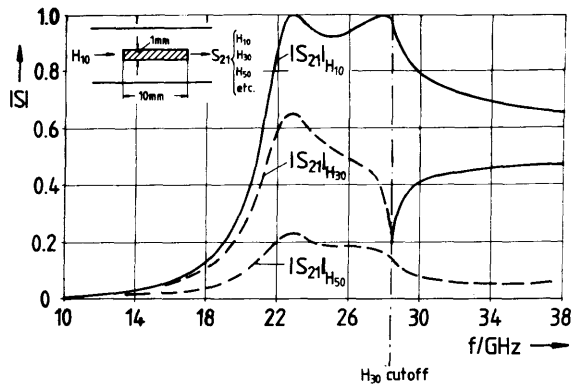

Fig. 3. Transition from a waveguide to a metal insert structure (Fig. 2(b)) and back to waveguide. Waveguide dimensions. a = 15·8 mm, b = 7·899 mm. Fundamental mode and first higher order mode scattering coefficients $|S_{21}|$ into the waveguide (right) if a H_{10}-mode is incident in the waveguide (left) as a function of frequency.

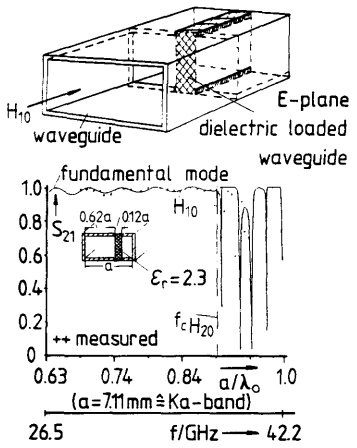

Fig. 4. Transition from a rectangular waveguide to a E-plane dielectric loaded waveguide. Scattering coefficient $|S_{21}|$ of the H_{10}-mode in the slab-line structure if a H_{10}-mode is incident in the waveguide as a function of frequency.

The good H_{10}-mode compatibility of E-plane structures is also demonstrated by the fundamental mode transmission coefficient $|S_{21}|$ of the transition waveguide to a waveguide with a dielectric slab mounted in the E-plane (Fig. 4), calculated according to Ref. 24. Below the H_{20}-mode cut-off frequency nearly all the energy is transmitted into the desired fundamental H_{10}-mode.

This is in contrast, for example to the common

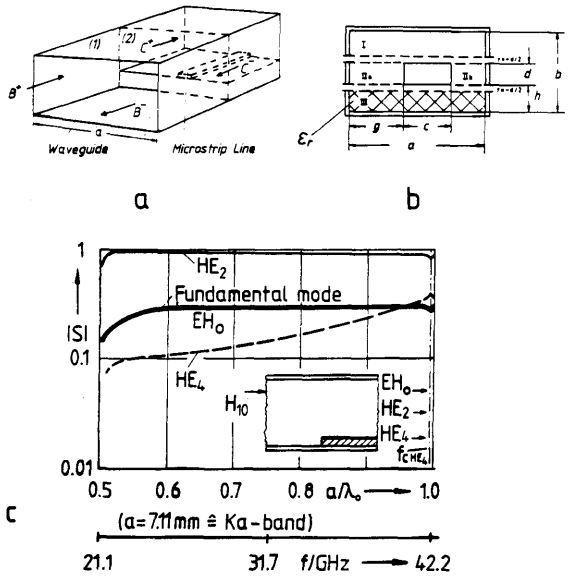

Fig. 5. Transition from a rectangular waveguide to a microstrip line. (a) View of the transition; (b) Cross-section of the shielded microstrip; (c) Transmission coefficient (scattering parameter $|S_{21}|$) of the step waveguide to microstrip as a function of frequency. Dimensions: b/a = 8/16, c/a = 3/16, d/a = 1/160, $g = (a-c)/2$, h/a = 1/16, ε_r = 9·7 (– · – · – cut-off frequencies).

microstrip-line where the substrate sheet is mounted in the H-plane. Figure 5 shows the magnitude of the transmission coefficients of the transition from a rectangular waveguide to the shielded microstrip-line calculated according to Refs. 25, 26. The coefficients are a function of normalized frequency a/λ_0 (a = width of the waveguide housing, λ_0 = wavelength in air). It is shown that the principal part of the transmitted power is transported by the first higher-order HE_2-mode and not by the commonly desired fundamental microstrip mode EH_0. This is because of the incoherence of the incident waveguide H_{10}-mode with the EH_0-mode where an E-mode portion dominates. It indicates that a direct waveguide implementation of microstrip lines is inappropriate. Since suitable tapered transitions (e.g. ridged waveguide tapers) are relatively complicated, for millimetre-wave integrated circuits E-plane structures are more adequate.

4 Optimization Procedure

For the computer optimization of the filters an error function is defined (Fig. 6)

$$F(\bar{x}) = \sum_{i=1}^{N_{stop}} (a_{s(min)}/a_{21}(f_i))^2 + \sum_{i=1}^{N_{pass}} (a_{21}(f_i)/a_{p(max)})^2 \stackrel{!}{=} \text{Min.}, \quad (6)$$

where the filter resonator and coupling section dimensions $\bar{x}$

$$\bar{x} = (l_1, l_2, l_3, \ldots, l_n) \quad (7)$$

are optimized to yield a minimum. Here, f_i are the frequency sample points, N_{stop} and N_{pass} are the number of sample points in stopband and passband respectively. A number of 20–30 frequency sample points, both in passband and stopband, has turned out to be sufficient.

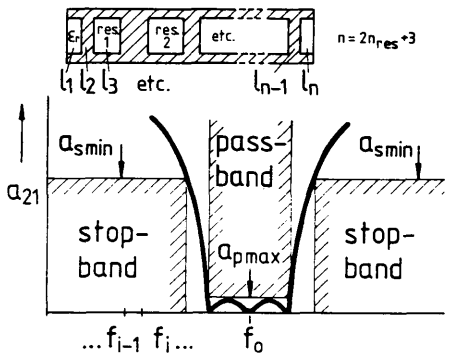

Fig. 6. Scheme for the computer optimization.

Values $a_{s(min)}$ and $a_{p(max)}$ are the given minimum stopband and maximum passband attenuation, respectively, and $a_{21} = 20 \log (1/|S_{21}|)$ is the insertion-loss at the frequency f_i, calculated according to Section 2. For first optimization results an expansion into five eigenmodes, see equation (3), is sufficient. The final results are proved by the expansion into twenty eigenmodes, and for the W-band filter in Fig. 11 into forty-five eigenmodes.

The initial values for l_2 to l_{n-1} (eqn. (7)) for the optimization procedure are chosen to be each $\lambda_0/2$, where λ_0 is the wavelength in air of the H_{10}-mode at the given midband frequency. Values l_1 and l_n, for the fin-line filter, are fixed by the given total substrate length L. For the metal insert filter l_1 and l_n are also initially chosen to be $\lambda_0/2$. In order to reduce the number of parameters the filters are assumed to be symmetrical with regards to the half of the total filter length.

A main optimization strategy parameter H and a secondary strategy parameter N influence[21] the alternation of the parameters $\bar{x}$ during the optimization process with a standard deviation $\sigma = H \cdot N$. Initial values for H and N are chosen to be $H = 0{\cdot}01$, $N = 1$.

Table 1

Computer-optimized design data for low-insertion-loss fin-line filters.

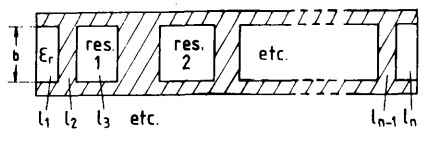

n = 2nres + 3

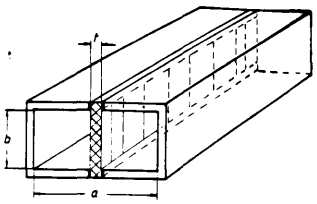

Frequency - band waveguide housing	Substrate material	Number of resonators n_{res}	Substrate thickness t	Copper cladding thickness	$l_1=l_n$ (mm)	$l_2=l_{n-1}$ (mm)	$l_3=l_{n-2}$ (mm)	$l_4=l_{n-3}$ (mm)	$l_5=l_{n-4}$ (mm)	$l_6=l_{n-5}$ (mm)	$l_7=l_{n-6}$ (mm)	Results see Fig.
X - band a = 22.86 mm b = 10.16 mm	RT/duroid 5880 ε_r = 2.22	4	1/32 "	17.5 µm	19.232	1.421	8.809	7.452	8.565	9.043		7 a
Ka - band a = 7.112 mm b = 3.556 mm	RT/duroid 5880 ε_r = 2.22	3	0.01 "	17.5 µm	19.77	0.705	3.75	3.9	3.75			8 a
E - band a = 3.10 mm b = 1.55 mm	Fused Silica (Quartz) ε_r = 3.8	3	0.220 mm	5 µm	11.016	0.336	1.457	1.462	1.459			10 a
E - band a = 3.10 mm b = 1.55 mm	Fused Silica (Quartz) ε_r = 3.8	5	0.220 mm	5 µm	5.595	0.305	1.477	1.333	1.493	1.554	1.488	10 b

During the optimization procedure the main strategy parameter H is altered as follows: For fewer than three trials, H is doubled, for more than three, H is halved; after a successful trial, H is left constant. If the deviation of the parameters $\bar{x}$ exceeds the limit $\lambda_0/2-0{\cdot}7\ \lambda_0/2 < x_i < \lambda_0/2+0{\cdot}7\ \lambda_0/2$, H is multiplied by 0·7. If the error function $F(\bar{x})$ is minimized three times by less than 1%, the result is interpreted as a local minimum. H is multiplied by 10^4. So the optimization process begins again for a different, perhaps better, parameter range, and the global minimum, if it differs from the already found local one, can be attained.

The secondary strategy parameter N is altered principally in the same manner. The altering factor for fewer than three trials is chosen to be 1·2, for more, 0·83. It is often convenient to adapt N to the individual parameters x_i: the resonator length variation should be less than the variation of the coupling sections, if, for

5 Results

Figure 7 shows the calculated and measured insertion-loss ($a = 20 \log (1/S_{21})$) in decibels as a function of frequency for four-resonator X-band pseudo-highpass filters. Considered for prototypes for television communication satellite front-ends, the filters have been optimized according to specifications given by H. Kolbe & Co., Bad Salzdetfurth, W.-Germany. Figure 7(a) relates to the fin-line type, and Fig. 7(b) to the metal insert type. The filters yield a measured minimum insertion loss of about 0·3 dB for the fin-line filter and 0·1 dB for the metal insert filter, respectively.

Three-resonator Ka-band filter results are indicated in Fig. 8. The corresponding measured minimum insertion-losses are 0·7 dB (fin-line, a), and 0·6 dB (metal insert, b). The insertion-loss curve of a three-resonator V-band metal insert filter is given in Fig. 9 (0·5 dB measured minimum insertion-loss).

Table 2
Computer-optimized design data for low-insertion-loss metal insert filters.

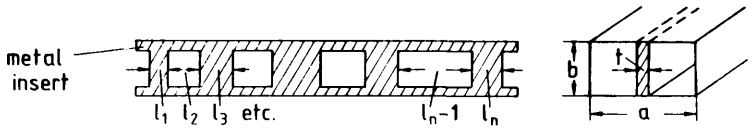

Frequency - band waveguide housing	Number of resonators	Insert thickness t (mm)	$l_1=l_n$ (mm)	$l_2=l_{n-1}$ (mm)	$l_3=l_{n-2}$ (mm)	$l_4=l_{n-3}$ (mm)	$l_5=l_{n-4}$ (mm)	$l_6=l_{n-5}$ (mm)	Results see Fig.
X - band a = 22.86 mm b = 10.16 mm	4	0.9	1.96	9.439	8.686	9.251	10.065		7 b
Ka - band a = 7.112 mm b = 3.556 mm	3	0.51	1.009	4.778	3.87	4.796			8 b
V - band a = 3.76 mm b = 1.88 mm	3	0.1	0.708	2.243	2.26	2.252			9
E - band a = 3.045 mm† b = 1.55 mm	3	0.1	0.613	1.911	1.978	1.917			10 c
E - band a = 3.1 mm b = 1.55 mm	4	0.1	0.617	1.92	1.92	1.927	2.1		10 d
E - band a = 3.1 mm b = 1.55 mm	5	0.1	0.615	1.918	1.91	1.925	2.1	1.93	10 e
W - band a = 2.54 mm b = 1.27 mm	4	0.05	0.845	1.438	2.355	1.439	2.579		11

† The a-dimension of this filter housing differs from the nominal E-band value by about −55 μm (construction error!). This results in a mid-band frequency shift of about +1 GHz which has been included in the computation of this filter.

instance, the ripple behaviour has to be improved while the mid-band frequency behaviour of the filter is already satisfactory.

On the average, every sixth optimization step was successful. The results of the optimization procedure are given in Table 1 for the fin-line filters, and in Table 2 for the metal insert filters. The total computing time for the optimization process of one set of filter parameters was about 10–30 min. A Siemens-7880 computer was used for the computations.

Figure 10 shows the insertion-loss behaviour of several E-band filters. In Figs. 10(a) and (b) three- and five-resonator fin-line filters are chosen; fused silica (quartz) is chosen for substrate material, because of its lower loss compared with RT/duroid 5880, used for the lower frequencies. The measured minimum insertion-losses are 1·3 dB, and 3 dB, for the three- and five-resonator filters, respectively. The corresponding values of the three- to five-resonator metal insert filters are 0·7, 2·3, 2·4 dB, respectively. The calculated insertion-loss of a four-

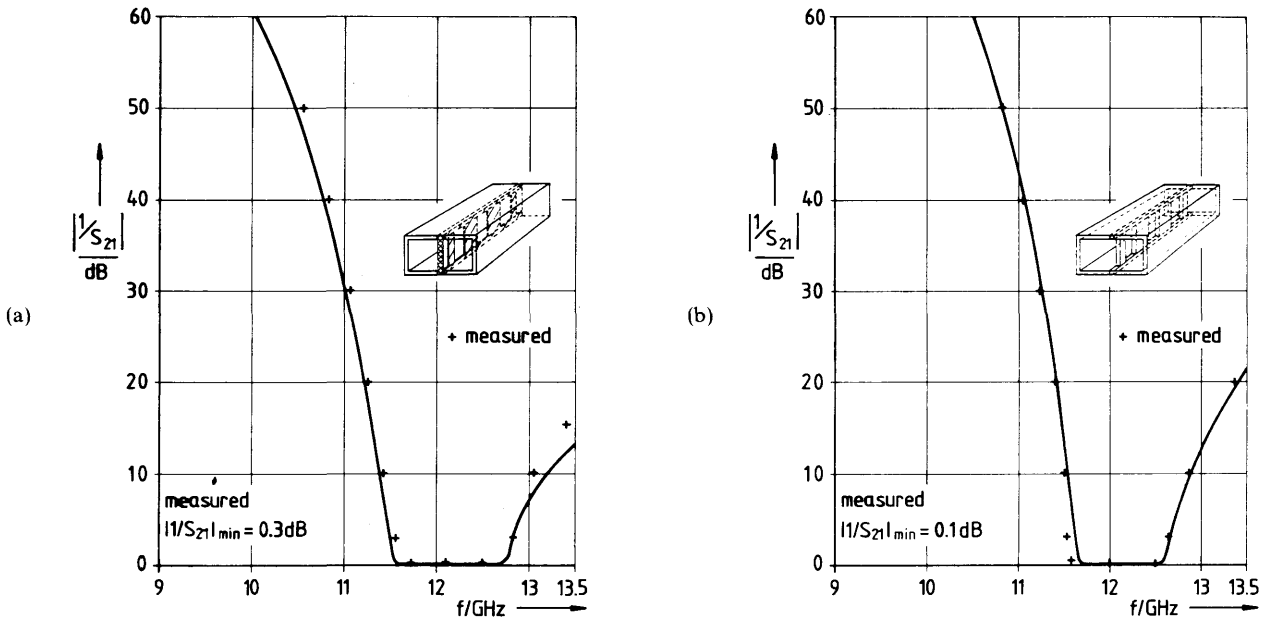

Fig. 7. Calculated and measured insertion-loss as a function of frequency of X-band pseudo-highpass filters suitable for TV-satellite-communication front-ends (data see Tables 1 and 2) (a) fin-line type; (b) metal insert type.

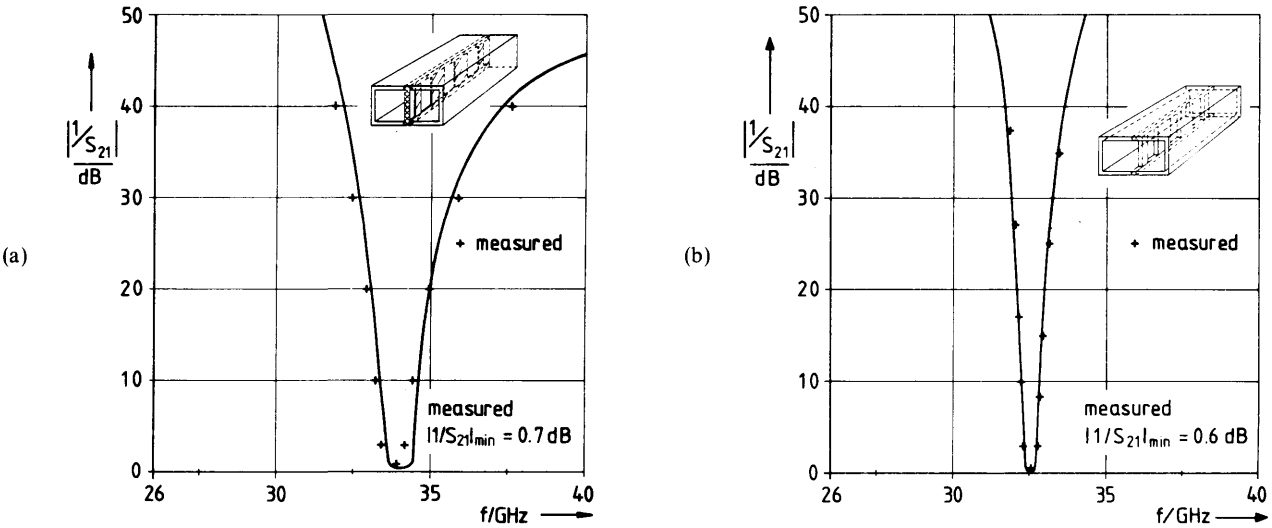

Fig. 8. Calculated and measured insertion-loss as a function of frequency of Ka-band filters (data see Table 1, 2). (a) fin-line type; (b) metal insert type.

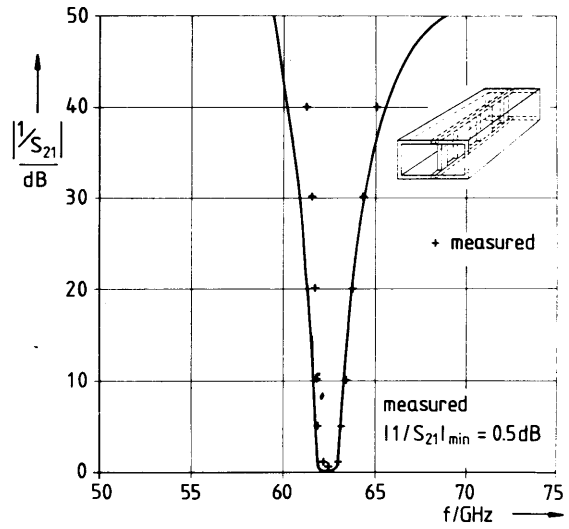

Fig. 9. Calculated and measured insertion-loss as a function of frequency of a V-band metal insert filter (data see Table 2)

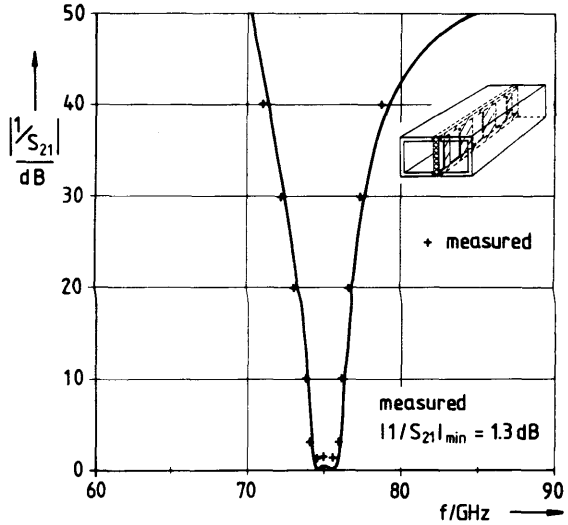

(a) three-resonator fin-line type

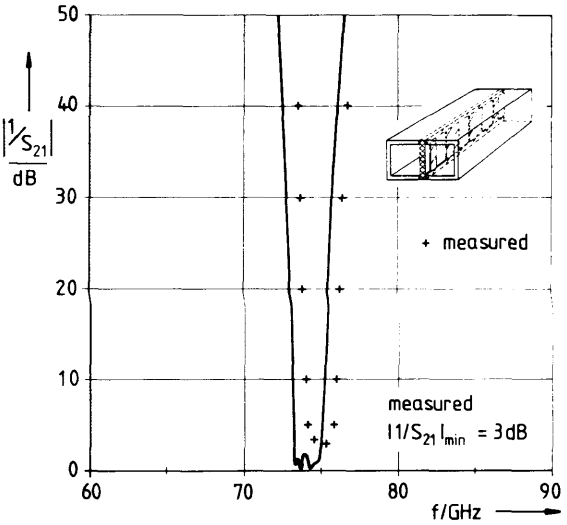

(b) five-resonator fin-line type

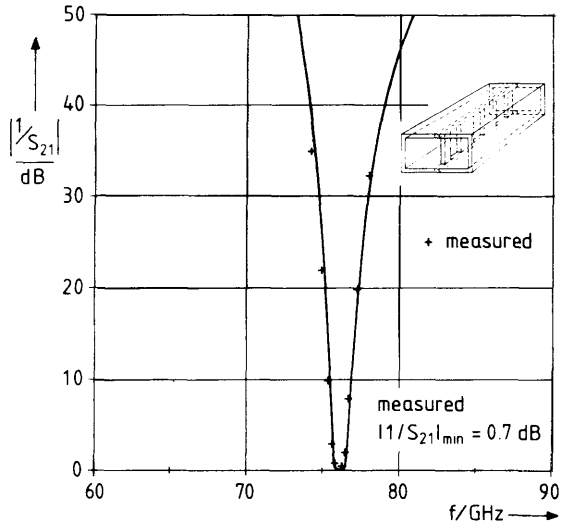

(c) three-resonator metal insert type

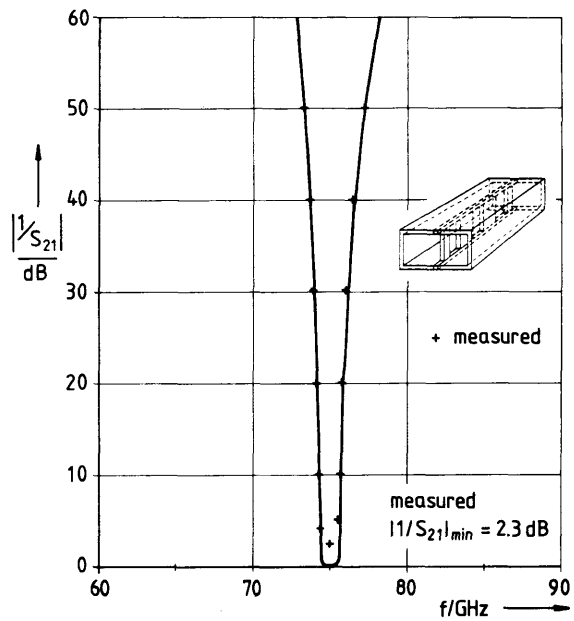

(d) four-resonator metal insert type

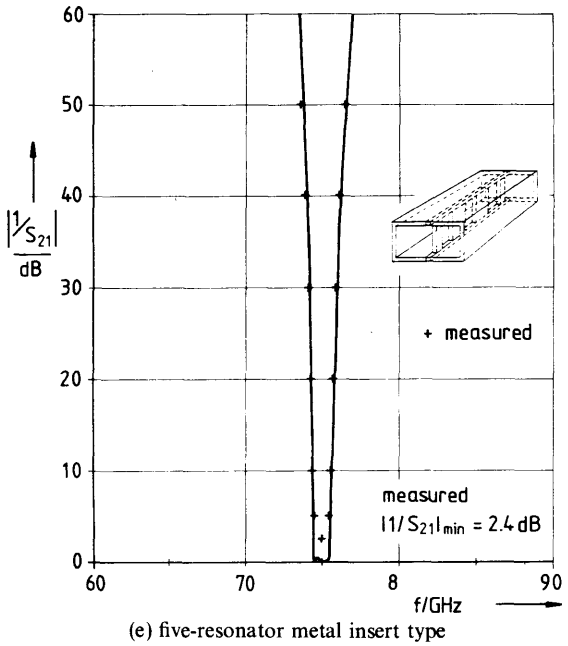

(e) five-resonator metal insert type

Fig. 10. Calculated and measured insertion-loss as a function of frequency of E-band filters (data see Tables 1 and 2).

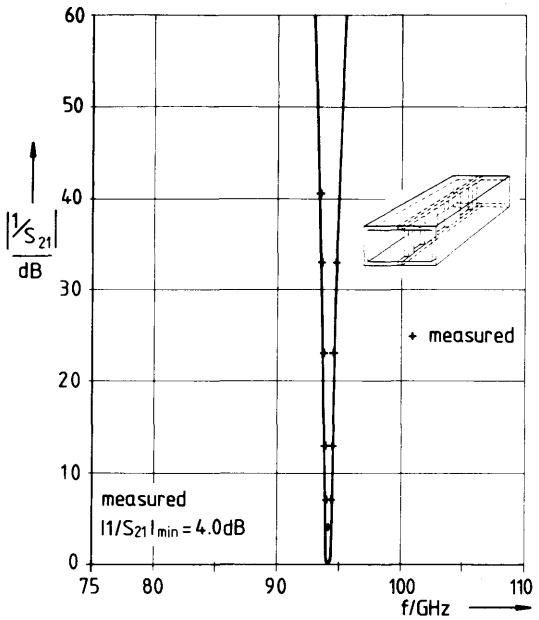

Fig. 11. Calculated insertion-loss as a function of frequency of a W-band metal insert filter.

resonator W-band metal insert filter is shown in Fig. 11. This filter is considered for application in millimetre-wave receiver systems and has been optimized according to specifications given by Dr Rembold, AEG-Telefunken, Ulm, W.-Germany. The measured minimum insertion-loss is 4·0 dB. Figure 12 shows the etched filter-structures of a fin-line and a metal insert E-band filter.

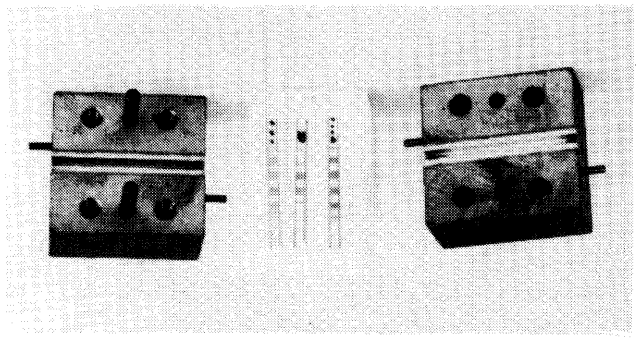

(a) fin-line type (two five-resonator and a three-resonator structure(s) on fused silica (quartz) substrate material).

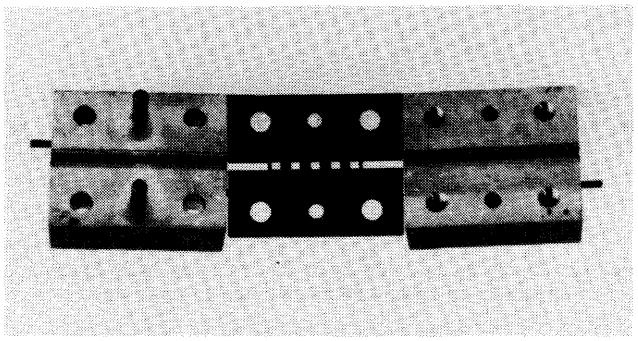

(b) metal insert type (five resonators).

Fig. 12. Etched E-band filter structures together with the corresponding waveguide housing.

The comparison of the measured and calculated filter responses shows a good coincidence between theory and practice. The slight frequency displacement between calculated and measured curves in some of the figures is caused by etching errors and production tolerances of the available material: copper cladding thickness about $\pm 2{\cdot}5$ μm (for the 17·5 μm thickness) and $\pm 0{\cdot}5$ μm (for the 5 μm thickness), substrate thickness about ± 20 μm, metal insert thickness about $\pm 5\%$. This has been checked by using the measured geometries of the filters in the theory.

6 Conclusions

A design theory has been described for low-insertion-loss fin-line and E-plane metal insert filters. The theory includes both higher-order mode interaction, and the finite thicknesses of dielectrics, metallic fins, and metal inserts.

The low-insertion-loss design is achieved by a large gap fin-line type, with a considerably higher unloaded Q compared with the common small gap design, and by a metal insert filter type requiring no supporting (lossy) dielectric substrate. The low-insertion-loss also results from the fact that no tapered transitions from waveguide to the E-plane printed circuit structures are required. For the fin-line, at lower frequencies, RT/duroid 5880 is used for substrate material. To reduce the losses fused silica (quartz) is chosen for higher frequencies because of its lower loss and surface roughness. The complete absence of supporting dielectrics, in the case of metal insert filters, achieves still lower insertion-losses.

A computer optimization leads to optimum design data for three-to five-resonator filters for X- to W-band application. Measurements verify the given theory. The low-insertion-loss E-plane integrated circuit filters combine the advantages of the low-loss design of common waveguide filters with the low-cost etching production technique of integrated circuit designs.

7 Acknowledgments

The E-band fin-line filters have been etched and measured and the V-, E- and W-band metal insert filters measured in the microwave laboratory of AEG-Telefunken, Ulm, W.-Germany. The authors are greatly indebted to Dr Rembold, the head of the laboratory, and the members of his staff, especially Dr Menzel, for this aid. Further, financial support for the W-band metal insert filter by AEG-Telefunken, via Dr Rembold, and for the X-band low-insertion-loss filters by Hans Kolbe & Co., Fuba, Bad Salzdetfurth, W.-Germany, via Dipl.-Ing. Begemann, is gratefully acknowledged as well as the permission for publication of results of the corresponding filter designs.

8 References

1 Meier, P. J., 'Equivalent relative permittivity and unloaded Q-factor of integrated fin-line', *Electronics Letters*, **9**, no. 7, pp. 162–3, April 1973.

2 Meier, P. J., 'Integrated fin-line millimeter components', *IEEE Trans. on Microwave Theory and Techniques*, **MTT-22**, pp. 1209–16, December 1974.

3 Meier, P. J., 'Millimeter integrated circuits suspended in the E-plane of rectangular waveguide', *IEEE Trans*, **MTT-26,** pp. 726–32, October 1978.
4 Mirshekar-Syahkal, D. and Davies, J. B., 'Accurate analysis of tapered planar transmission lines for microwave integrated circuits', *IEEE Trans.*, **MTT-29,** pp. 123–8, February 1981.
5 Saad, A. M. K. and Schünemann, K., 'A simple method for analyzing fin-line structures', *IEEE Trans.*, **MTT-26,** pp. 1002–7, December 1978.
6 Saad, A. M. K. and Schünemann, K., 'Design and performance of fin-line bandpass filters', Proc. 9th European Microwave Conf., Brighton, 1979, pp. 397–401.
7 Hennawy, H. E. and Schünemann, K., 'Analysis of fin-line discontinuities, Proc. 9th European Microwave Conf., Brighton, 1979, pp. 448–52.
8 Hoffmann, H., 'Dispersion of planar waveguides for millimeter-wave application', *Arch. Elek. Ubertragung*, **31,** pp. 40–4, 1977.
9 Beyer, A., 'Analysis of the characteristics of an earthed fin-line', *IEEE Trans.* **MTT-29,** pp. 676–80, July 1981.
10 Beyer, A. and Wolff, I., 'A solution of the earthed fin-line with finite metallization thickness', 1980 IEEE MTT-S Int. Microwave Symp. Digest Washington, DC, pp. 258–60.
11 Schmidt, L. P., Itoh, T. and Hofmann, H., 'Characteristics of unilateral fin-line structures with arbitrarily located slots', *IEEE Trans.*, **MTT-29,** pp. 352–55, April 1981.
12 Arndt, F., Bornemann, J., Grauerholz, D. and Vahldieck, R., 'Theory and design of low-insertion loss fin-line filters', *IEEE Trans.*, **MTT-30,** pp. 155–63, February 1982.
13 Arndt, F., Bornemann, J., Grauerholz, D. and Vahldieck, R., 'Low-insertion loss fin-line filters for millimetre-wave applications', Proc. 11th European Microwave Conf., Amsterdam, 1981, pp. 309–14.
14 Adelseck, B., Callsen, H., Hofmann, H., Meinel, H. and Rembold, B., 'Neue Millimeterwellenkomponenten in quasiplanarer Leitungstechnik', *Frequenz*, **35,** pp. 118–23, May 1981.
15 Konishi, Y. *et al.*, 'Simplified 12-GHz low-noise converter with mounted planar circuit in waveguide', *IEEE Trans.*, **MTT-22,** pp. 451–4, April 1974.
16 Reindel, J., 'Printed wg circuits trim component costs', *Microwaves*, pp. 60–63, October 1980.
17 Meier, P. J., 'Two new integrated-circuit media with special advantages at millimeter wavelength', Digest IEEE 1972 G-MTT Symp., May 1972, pp. 221–3.
18 Konishi, Y. and Uenakada, K., 'The design of a bandpass filter with inductive strip-planar circuit mounted in waveguide', *IEEE Trans.* **MTT-22,** pp. 869–73, October 1974.
19 Tajima, Y. and Sawayama, Y., 'Design and analysis of a waveguide-sandwich microwave filter', *IEEE Trans.*, **MTT-22,** pp. 839–41, September 1974.
20 Vahldieck, R., Bornemann, J., Arndt, F. and Grauerholz, D., 'Optimized waveguide E-plane metal insert filter for millimeter-wave applications', to be published.
21 Schmiedel, H., 'Anwendung der Evolutionsoptimierung auf Schaltungen der Nachrichtentechnik', *Frequenz*, **35,** pp. 306–10, November 1981.
22 Fletcher, R. and Powell, M. J. D., 'A rapidly convergent descent method for minimization', *Computer J.*, **6,** pp. 163–8, 1963.
23 Collin, R. E., 'Field Theory of Guided Waves', chap. 1.6., pp. 22–7, and chap. 6.2, pp. 232–44. (McGraw-Hill, New York, 1960).
24 Engel, W. and Kruse, J., 'Berechnung der Streumatrix verschiebbarer dielektrischer Stoffeinsätze in Rechteckholleitern', Diploma thesis, University of Bremen, 1978.
25 Arndt, F. and Paul, U., 'The reflection definition of the characteristic impedance of microstrips', *IEEE Trans.*, **MTT-28,** pp. 724–31, August 1979.
26 Paul, U., 'Berechnung des sprunghaften Übergangs vom Rechteckhohlleiter zur geschirmten Streifenleitung mit homogenem sowie mit inhomogenem Dielektrikum', Dr.-Ing. thesis, University of Bremen, 1976.

9 Appendix

Abbreviations in equation (3)

$$\begin{bmatrix} f^{I} \\ f^{II} \\ f^{III} \\ f^{IV} \end{bmatrix} = \begin{bmatrix} x \\ d-(e/2)-x \\ a-x \\ x \end{bmatrix}$$

$$\begin{bmatrix} p^{I} \\ p^{II} \\ p^{III} \\ p^{IV} \end{bmatrix} = \begin{bmatrix} a \\ d-c-e \\ a-(d+(e/2)) \\ c-e/2 \end{bmatrix}$$

$$\begin{bmatrix} k_{zm}^{I2} \\ k_{zm}^{II2} \\ k_{zm}^{III2} \\ k_{zm}^{IV2} \end{bmatrix} = k^{v2} - \begin{bmatrix} (m\pi/a)^2 \\ (m\pi/p^{II})^2 \\ (m\pi/p^{III})^2 \\ (m\pi/p^{IV})^2 \end{bmatrix}, \quad k^{v2} = \omega^2 \mu_0 \varepsilon_v.$$

Coupling integrals

$$H_{mn} = \int_{x=c+e/2}^{d-e/2} \sin\left(\frac{m\pi}{a}x\right) \sin\frac{n\pi}{d-c-e}\left(d-\frac{e}{2}-x\right) dx$$

$$H_{mk} = \int_{x=d+e/2}^{a} \sin\left(\frac{m\pi}{a}x\right) \sin\frac{k\pi}{a-d-\frac{e}{2}}(a-x)\, dx$$

$$H_{ml} = \int_{x=0}^{c-e/2} \sin\left(\frac{m\pi}{a}x\right) \sin\frac{l\pi}{c-\frac{e}{2}}(x)\, dx.$$

Manuscript received by the Institution on 7th June 1982
(Paper No. 2054/CC 360)